Supporting information: How microstructures, oxide layers, and charge transfer reactions influence double layer capacitances. Part 1: impedance spectroscopy and cyclic voltammetry to estimate electrochemically active surface areas (ECSAs)

Maximilian Schalenbach* [a], Victor Selmert [a,b], Ansgar Kretzschmar [a], Luc Raijmakers [a], Yasin Emre Durmus [a], Hermann Tempel [a], Rüdiger-A. Eichel [a,b]

[a] Fundamental Electrochemistry (IEK-9), Institute of Energy and Climate Research, Forschungszentrum Jülich, Wilhelm-Johnen-Straße, 52425 Jülich, Germany

[b] Institute of Physical Chemistry, RWTH Aachen University, 52062 Aachen, Germany

** Corresponding author: m.schalenbach@fz-juelich.de*

Contents

1 Cell used for the electrochemical measurements

Figure S1 shows an illustration of the cell used for the electrochemical impedance spectroscopy (EIS) and cyclic voltammetry (CV) measurements. The cell consists of four main parts: (i) The main body, made of a milled polypropylene (PP) cylinder, has as a compartment for the working electrode (WE), the counter electrode (CE), and the reference electrode (RE), respectively. The WE is placed on the ground of the main body. The compartment is connected by a 4 mm hole to the WE compartment. A 4 mm PTFE tube with a tapered shape (one side thermally widened) was pressed into the hole, making a leak tight connection between the different compartments. This PTFE tube serves as a Luggin Capillaries, to bring the CE closer to the WE. The cell can be purged with nitrogen or argon via a glass frit or a hole at ride of the main body (covered in the illustration in Figure S1). (ii) A cap, which serves as a sealing to avoid that the electrolyte of the working electrode department meets air. (iii) A stainless-steel base plate, to which with four screws the main body was pressed. (iv) A PP specimen holder for the usage of carbon felt samples. This component was left out for the usage of plane samples, which directly pressed onto the stainless-steel base plate.

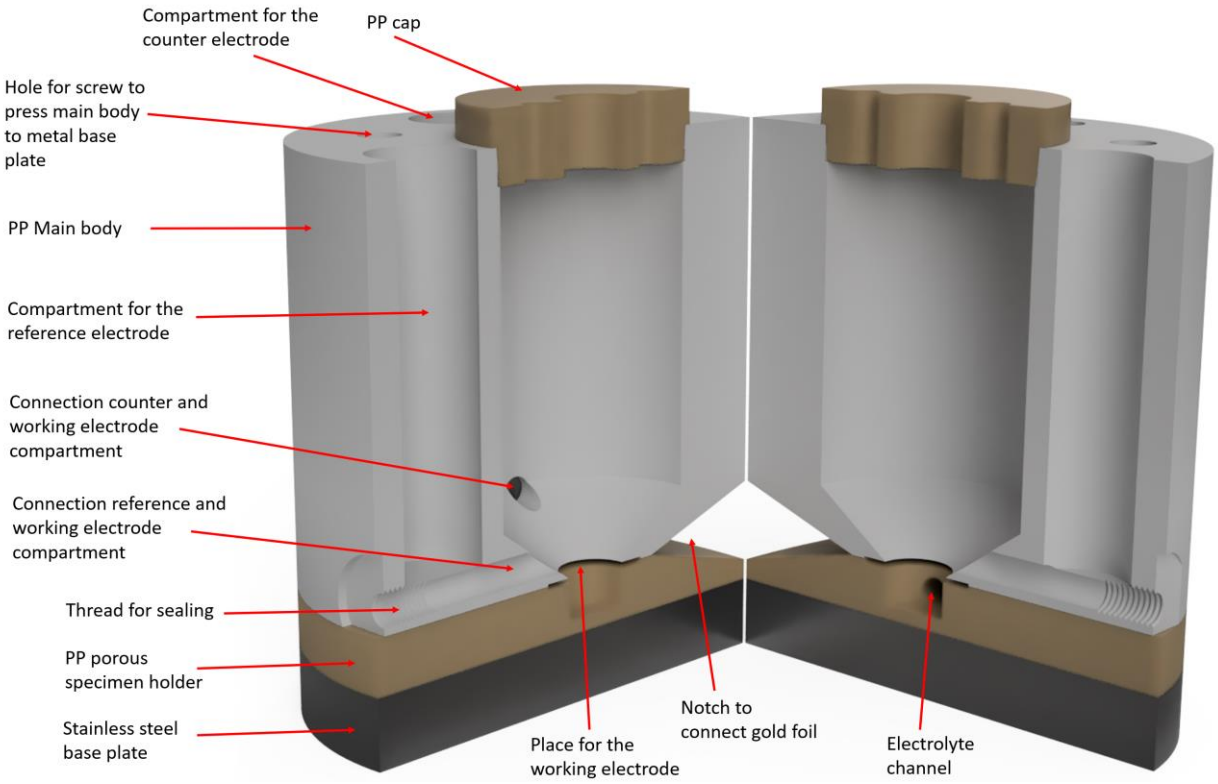

Figure S1: Illustration of the cell used for the measurements.

Figure S2 shows a schematic sketch on the sealing concept for the porous specimen. A gold foil was used to contact the porous carbon felts. The porous carbon specimen with 12 mm diameter were punched out with a round shaped iron tool and laid into a punched-out PTFE sealing. This PTFE sealing sealed the interface between the PP porous specimen holder and the gold foil. A rubber sealing (ethylene propylene diene monomer rubber) was used between the gold foil and the PP main body. For the usage of plane specimen, only the rubber sealing was used.

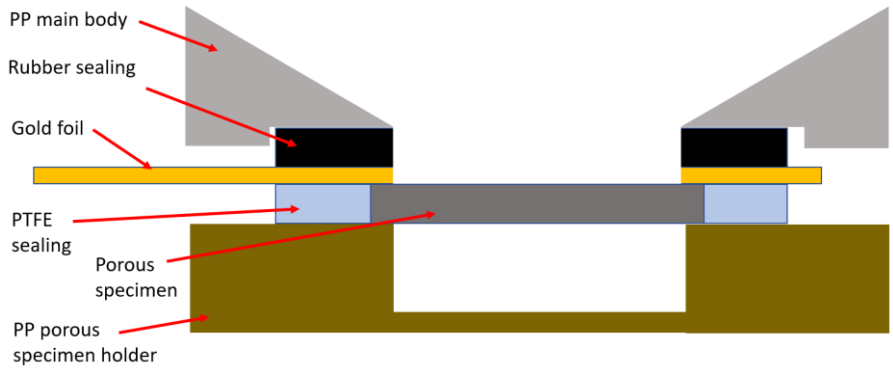

Figure S2: Sealing concept used for the porous specimen.

Prior to the measurements, the cell was cleaned in an oxalic acid solution to remove metal ions. After rinsing the cell with ultrapure water, it was cleaned in a diluted mixture of sulfuric acid and hydrogen peroxide. After these cleaning steps, the cell was thoroughly cleaned with ultrapure water to remove any residuals of the cleaning chemicals.

2 SEM pictures

Figure S3 shows the SEM pictures of the pinholes and craters on the glassy carbon electrode in two different resolutions. The glassy carbon sample shows craters, which may have large surface areas.

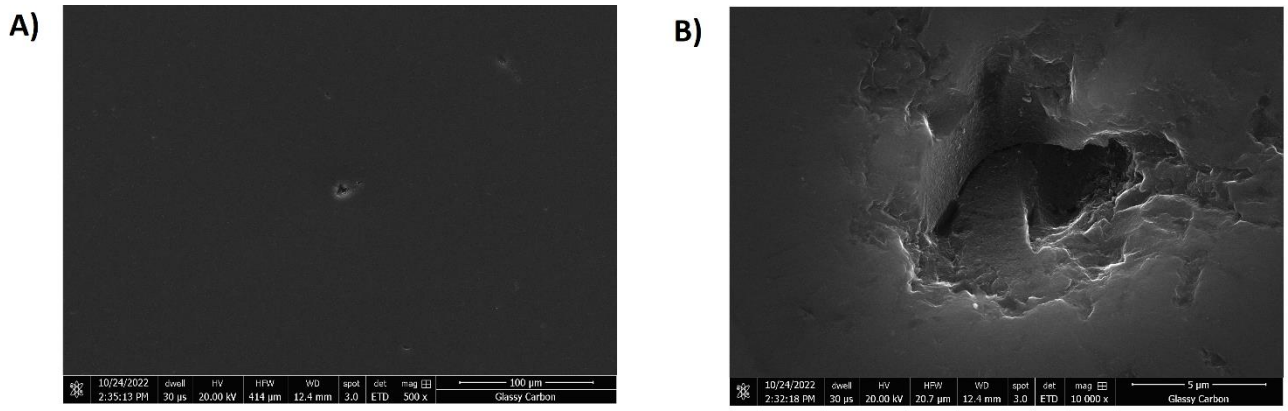

Figure S3: SEM pictures of the glassy carbon type 1 electrode.

3 Hg porosity measurements on the Freudenberg E35 carbon fleece

Figure S4 shows Hg porosity measurements on the Freudenberg E35 carbon fleece. These data show no significant increase of the pore volume below 1 µm. The electrochemical measurements also did not show any features below the relaxation frequency that could indicate micro-porosity.

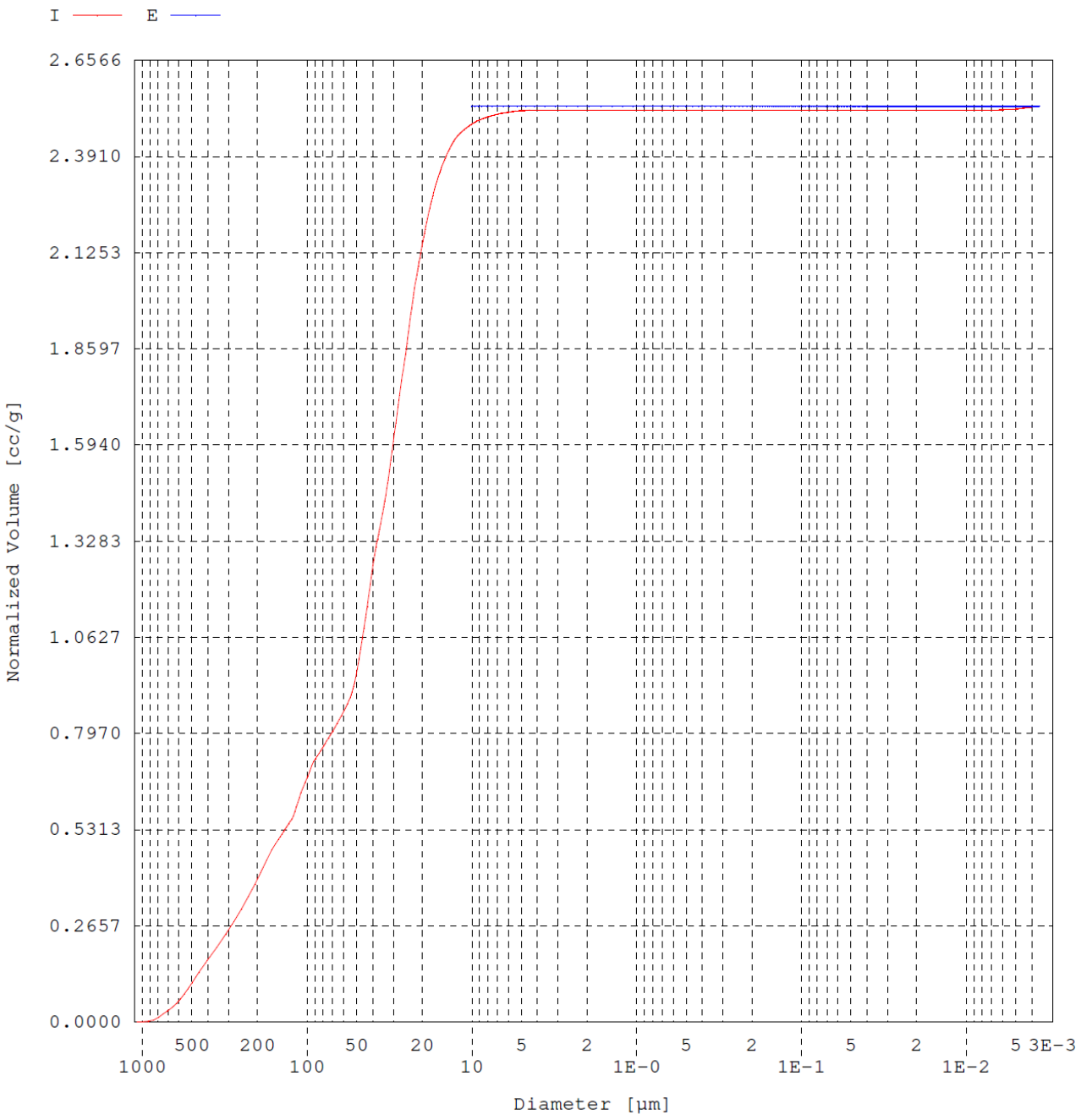

Figure S4: Hg-porosity measurements on the Freudenberg E35 carbon fleece electrode. The data does not show any increase of the pore volume below 1 µm.

4 BET measurements and evaluation

The gas adsorption isotherms exhibit a Type II shape for all samples, as is expected for non-micro-porous samples. The BET area was calculated from the data in the relative pressure range from 0.1 to 0.3. The relative pressure is defined as the absolute pressure divided by the saturation vapor pressure at the measurement temperature.

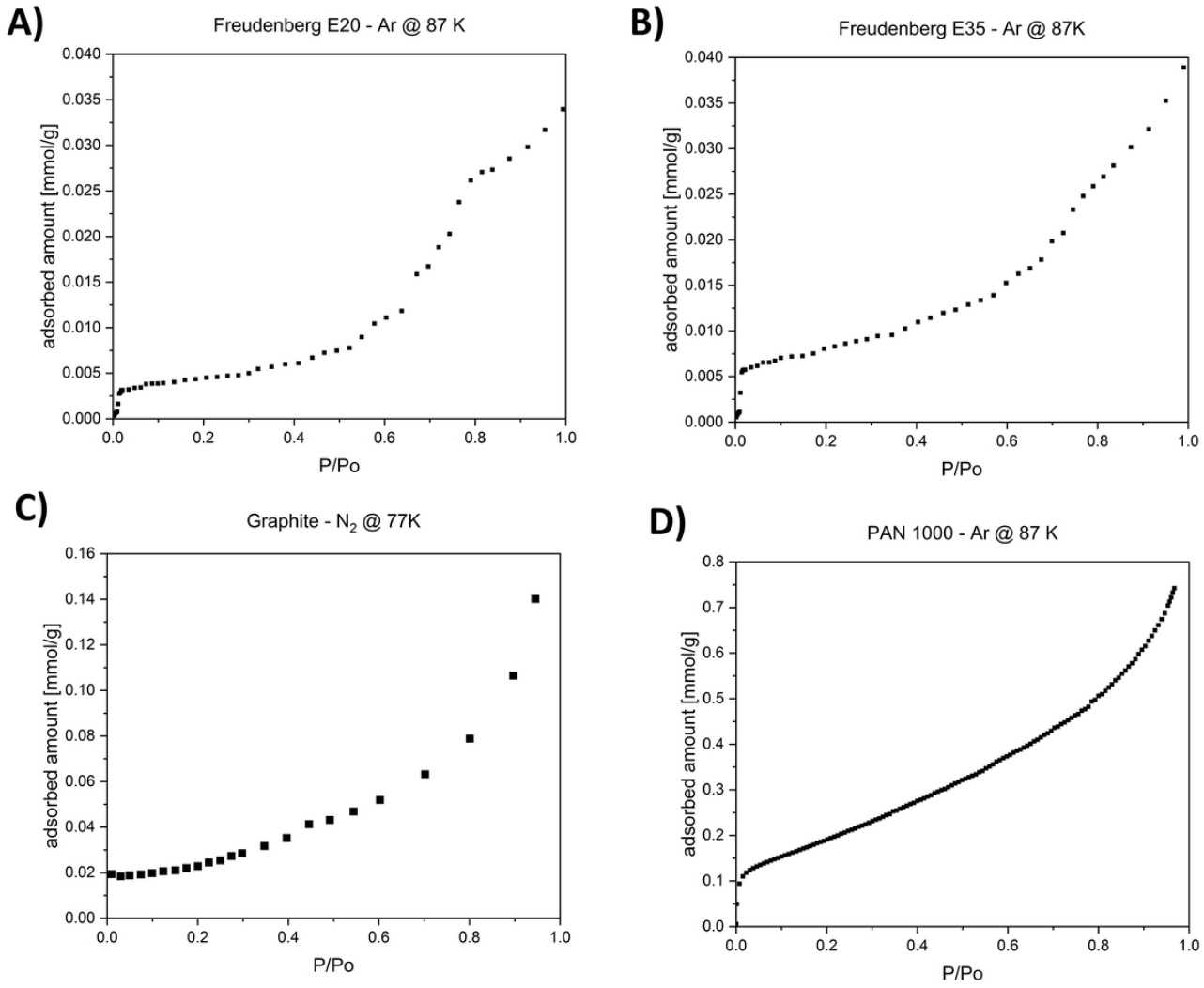

Figure S5: Adsorption isotherms of argon at 87 K on Freudenberg E20 (a), Freudenberg E35 (b), PAN 1000 (c) and nitrogen at 77 K on Graphite (d).

Consisting of fibers with diameters in the range of 200 nm, the sample PAN 1000 shows the highest uptake in this range, corresponding to a surface area of 14.8 m²/g. For the samples E20, E35 and the graphite, the BET areas are significantly lower, reaching values between 0.3 m²/g and 0.9 m²/g. The uncertainties of the measurements of the Freudenberg carbon felts and the graphite plate were estimated to ± 15 %, since the BET surface area determination with argon and nitrogen is close to its limits at such low specific surface areas. This estimation of an uncertainty of 15 % is based on the standard deviation of a measurement series with reference samples comparable in surface area. The measurement error of the PAN specimen pyrolyzed at 1000°C is similarly estimated to 5%, which is significantly more precise that of the other specimen due to a larger specific surface area.

*Table 1: Data for the BET measurements. * For graphite, N2 was chosen as adsorptive, since the sample cell for liquid nitrogen is larger, and therefore, allows to reduce the uncertainty by measuring a higher amount of sample.*

Sample	**Adsorptive**	**BET surface area**
Freudenberg E20	Ar	0.6 m²/g
Freudenberg E35	Ar	0.9 m²/g
PAN 1000°C	Ar	14.8 m²/g
Graphite	N_2*	0.3 m²/g

5 Gold contact for porous specimens

Figure S6 show the impedance spectrum and capacitance dispersion of the gold contact foil from Figure S2. These data were recorded in 1 M perchloric acid without using a porous specimen but with the contacting shown in Figure S2. The capacitance of the foil is orders of magnitude lower than those of the porous specimen, for which its contribution to the measurements is neglected.

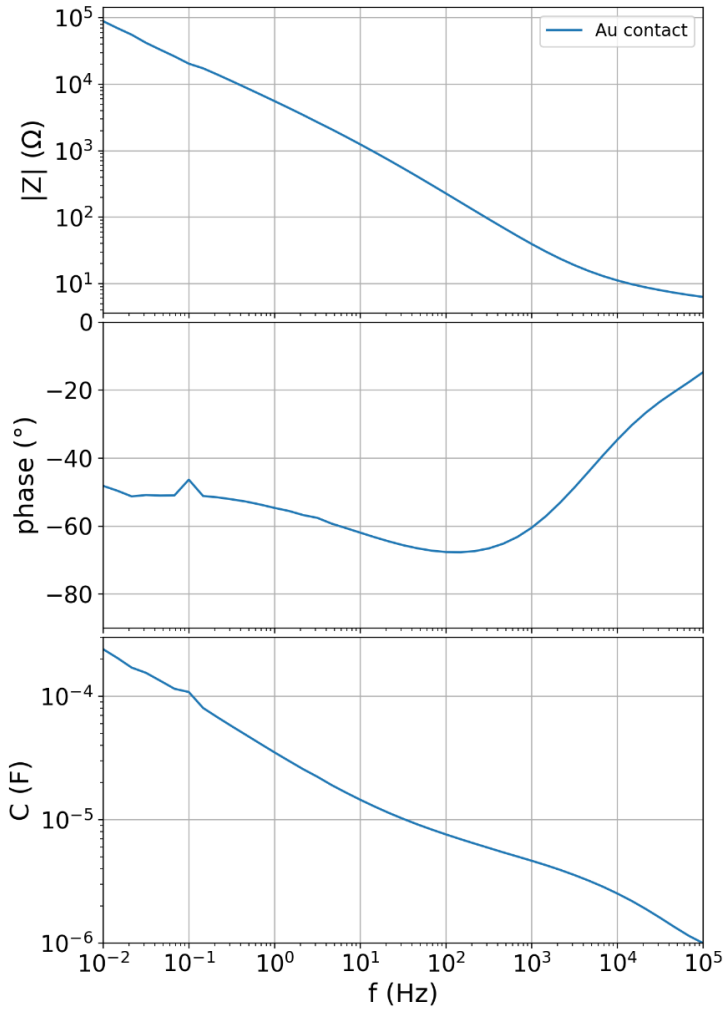

Figure S6: Impedance spectrum and capacitance dispersion of the gold contact foil from Figure S2.

6 Glassy carbon type 2 electrode in nitrogen and oxygen purged 1 M perchloric acid

Figure S7 shows the impedance data of the glassy carbon type 2 electrode in oxygen and nitrogen purged 1 M perchloric acid. As the data with the two different gas supplies does not show any significant difference, oxygen in the electrolyte (impurities or deliberately introduced) does not introduce a significant charge transfer reaction.

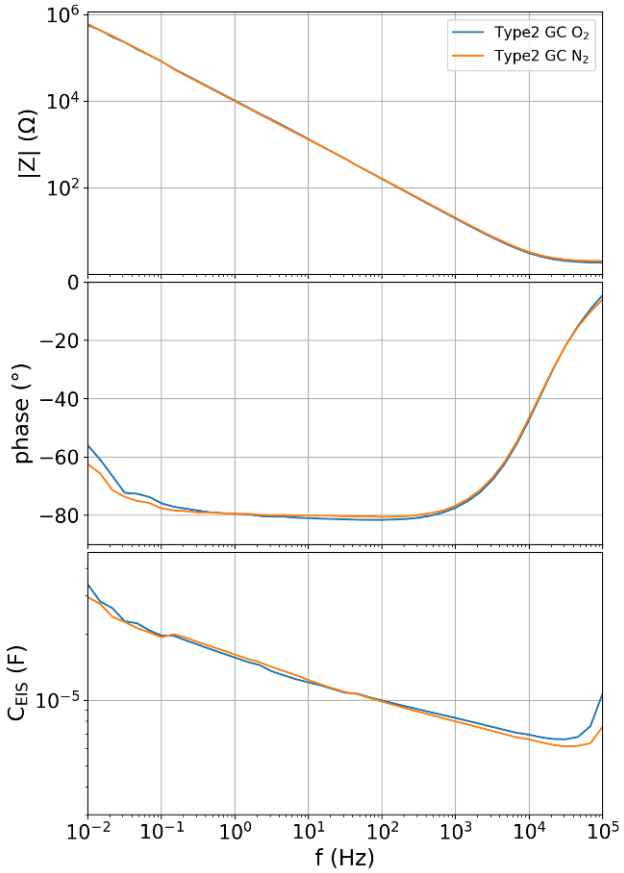

Figure S7: Impedance spectrum of the glassy carbon type 2 electrode in nitrogen and oxygen purged 1 M perchloric acid.

7 Different amounts of stacked Freudenberg E35 carbon fleeces

Figure S8 shows the impedance spectra and capacitance dispersions of different amounts of stacked Freudenberg E35 carbon fleeces. Some key parameters of the data of Figure S8 are condensed in Table S2 and used in Figure 5B of the article to show the proportionality of the capacitance as a function of the surface area.

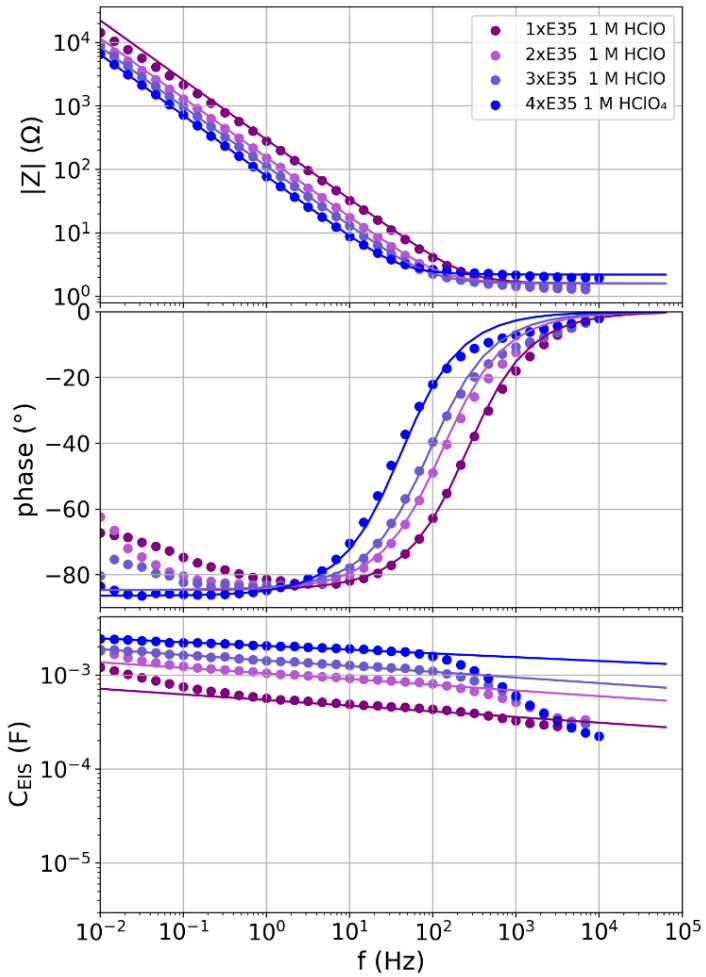

Figure S8:Impedance spectra and capacitance dispersion of stacks of the porous carbon fleece Freudenberg E35.

Table S2: Table for the fit parameters for the specimens presented in Figure S8 and S9.

	$f_{-45°}$ (Hz)	f_r (Hz)	$C_{-45°}$ (µF)	A (cm²)	$\tilde{C}_{spec}$ (µF/cm²)	$I_{bypass,CV}$ (nA)	$I_{bypass,PS}$ (nA)	$R_{s,fit}$ (Ω)	n_{fit}	ξ_{fit} (Ω Hz^n)
1xE35 1 M HClO	234	244	408	109	3.75	3230	835	1.6	0.94	1661
2xE35 1 M HClO	121	125	794	225	3.52	23577	8489	1.6	0.94	867
3xE35 1 M HClO	80	88	1128	345	3.27	34153	23296	1.6	0.94	631
4xE35 1 M $HClO_4$	34	40	1791	462	3.88	10078	194	2.2	0.96	456
PAN 1 M $HClO_4$	6.1	7.0	7545	2017	3.74	9959	-5745	3	0.96	124
Quartz PAN 1 M $HClO_4$	10267	14539	3.7	1.0	3.65	-478	-817	3	0.82	40000

8 Pyrolyzed PAN specimen

Figure S9 shows impedance spectra and capacitance dispersions of the pyrolyzed PAN carbon felt specimen and a porous quartz glass frit with a PAN coating pyrolyzed at 1000°C. The latter specimen illustrates how limiting electron conducting affects the response.

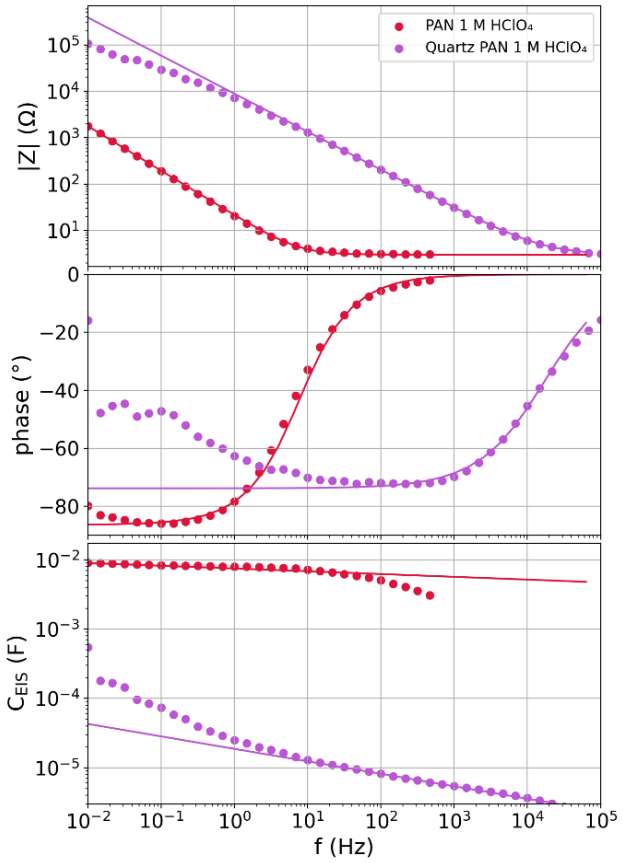

Figure S9: Impedance spectra of the PAN carbon felt electrode and the porous quartz glass specimen with PAN coating.

9 EIS data of the examined electrodes as Nyquist plots

Figure S10 shows Nyquist plots of the impedance data of the discussed specimen. As the capacitance is not directly visible in the Nyquist plots, the Bode representation in combination with the capacitance dispersion was preferred in the article.

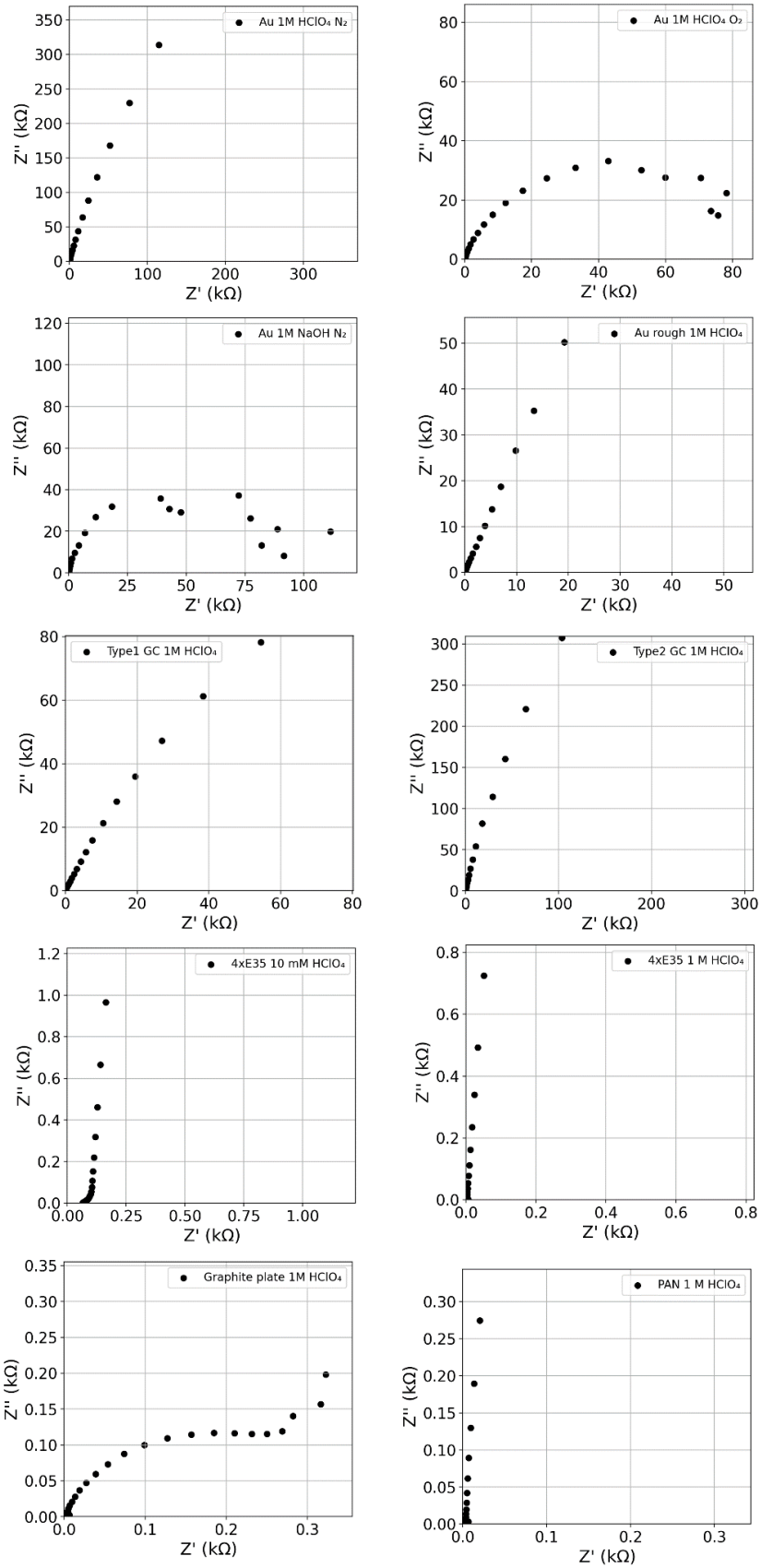

Figure S10: Nyquist plots of the EIS data on the different specimen discussed in the article.

10 CV data of the examined electrodes

Figure S11 shows the CV data of the examined specimen, using the ratio of measured current to scan rate to obtain the dimension of a capacitance.

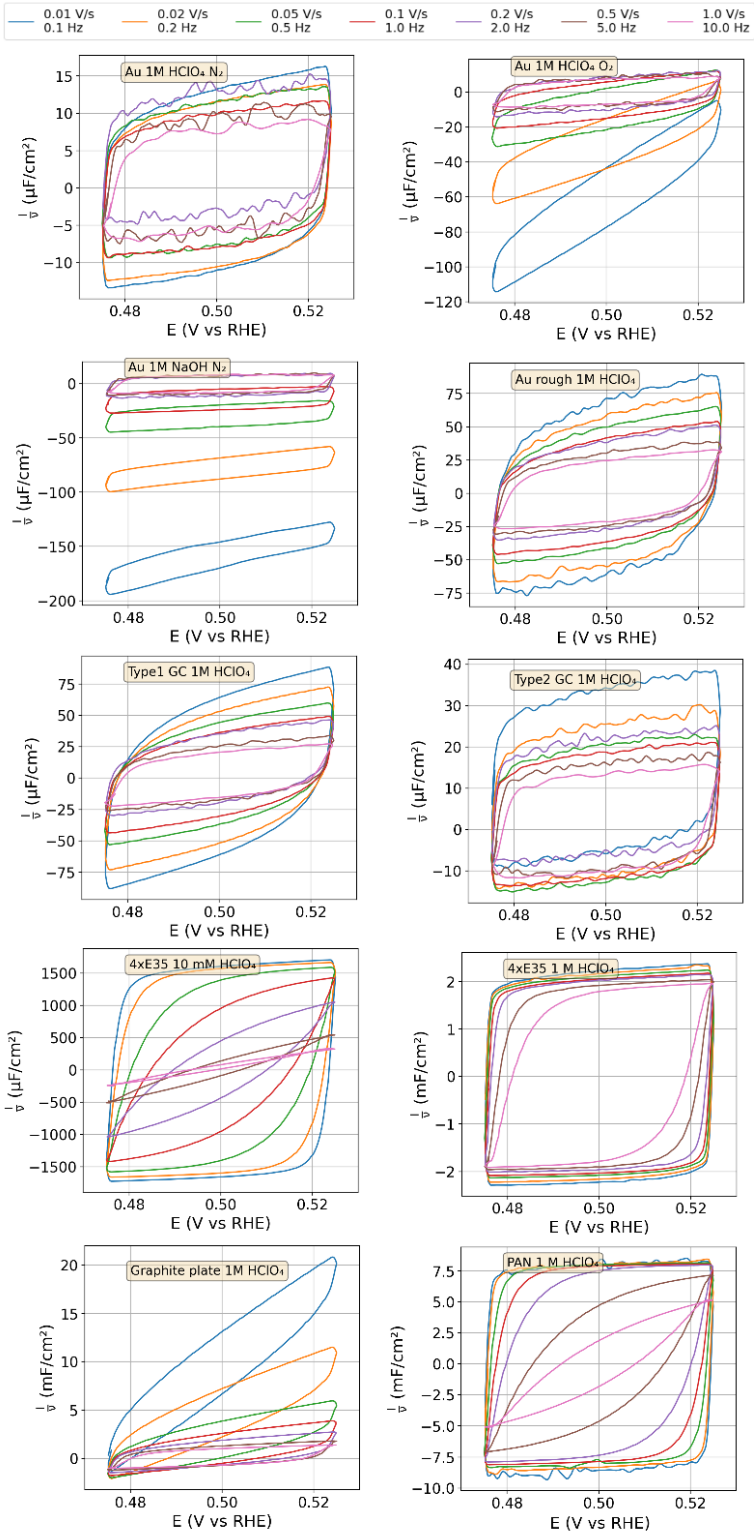

Figure S11: CV data of the discussed electrodes.

11 CV data of gold and carbon specimens between 0 and 0.6 V

Figure S12 shows the CV data of gold and carbon specimens in a potential range between 0 and 0.6 V.

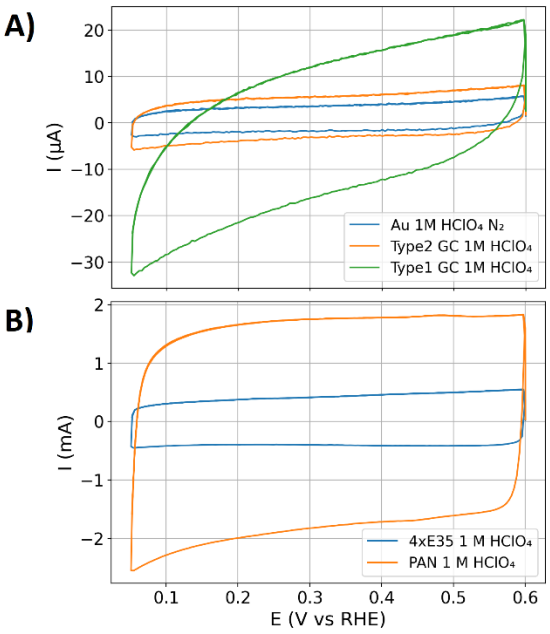

Figure S12: CV data of plane specimen (A) and porous carbon fleeces (B) obtained with a scan rate of 0.2 V/s.

12 EIS data and bypass currents of the examined Ti, Ru, Pt, and Ni specimens

Figure S13, S14, S15, and S16 show impedance spectra and capacitance dispersions on the Ti, Ru, Pt, and Ni specimen. From the potential increase ramps (see definition from the article) the measurements at three different electrode potentials are graphed. Figure S17 shows the bypass current of each of the metal specimen during the potential increase ramps (recorded shortly before the impedance measurements started).

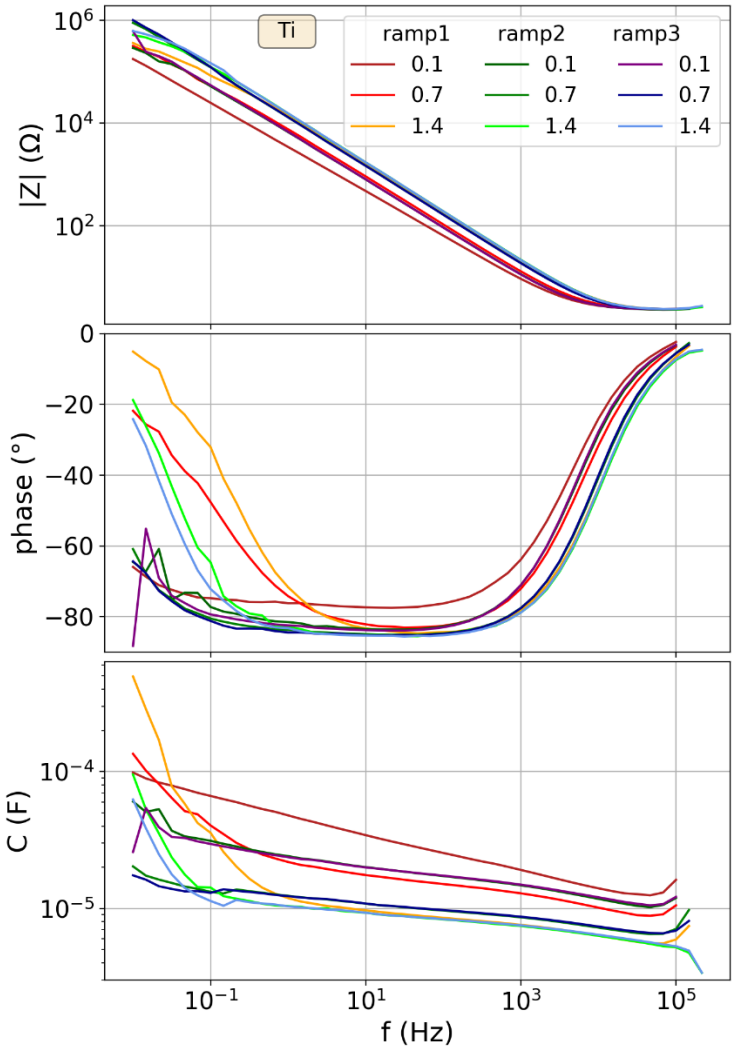

Figure S13: Nine impedance spectra and capacitance dispersions of the Ti electrode, three for each potential ramp at potentials of 0.1, 0.7 and 1.4 V vs RHE.

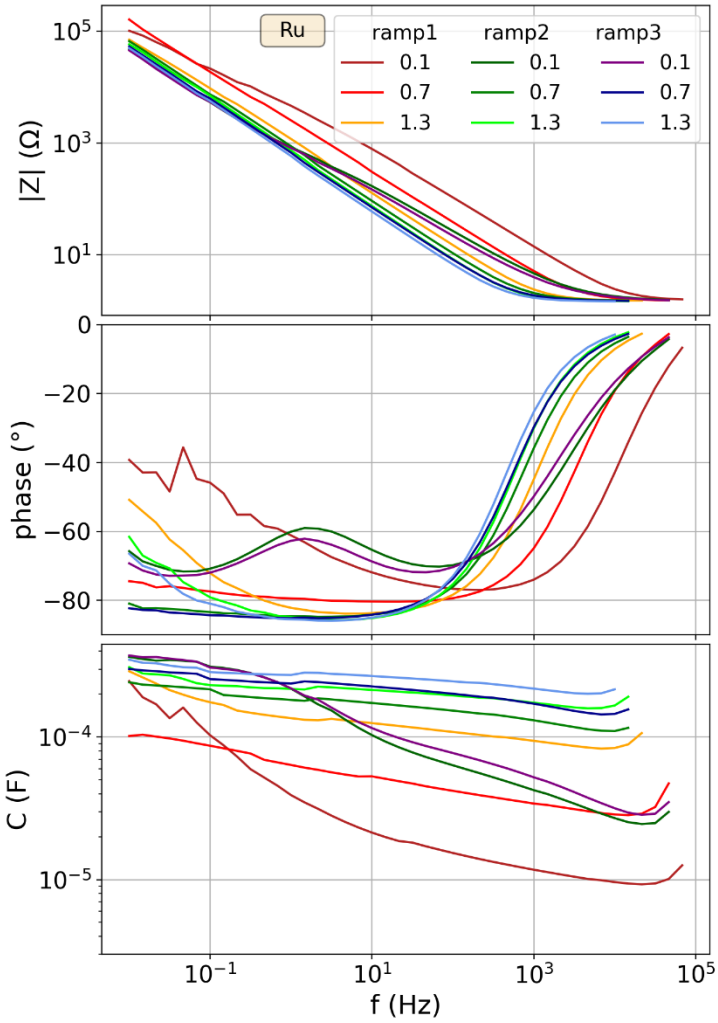

Figure S14: Nine impedance spectra and capacitance dispersions of the Ru electrode, three for each potential ramp at potentials of 0.1, 0.7 and 1.3 V vs RHE.

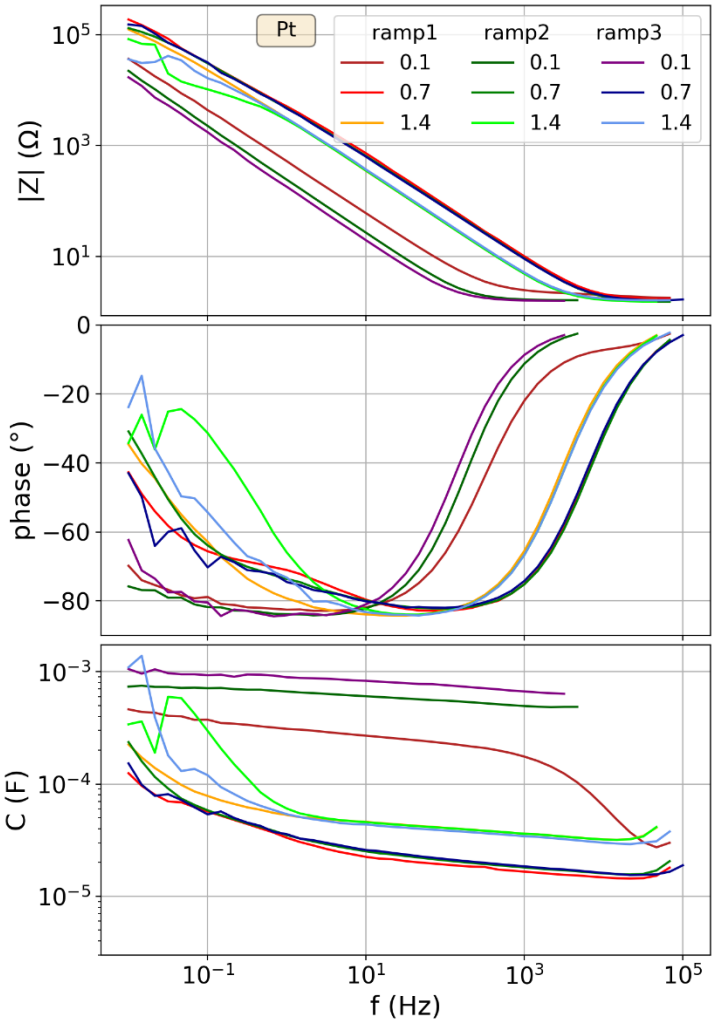

Figure S15: Nine impedance spectra and capacitance dispersions of the Pt electrode, three for each potential ramp at potentials of 0.1, 0.7 and 1.4 V vs RHE.

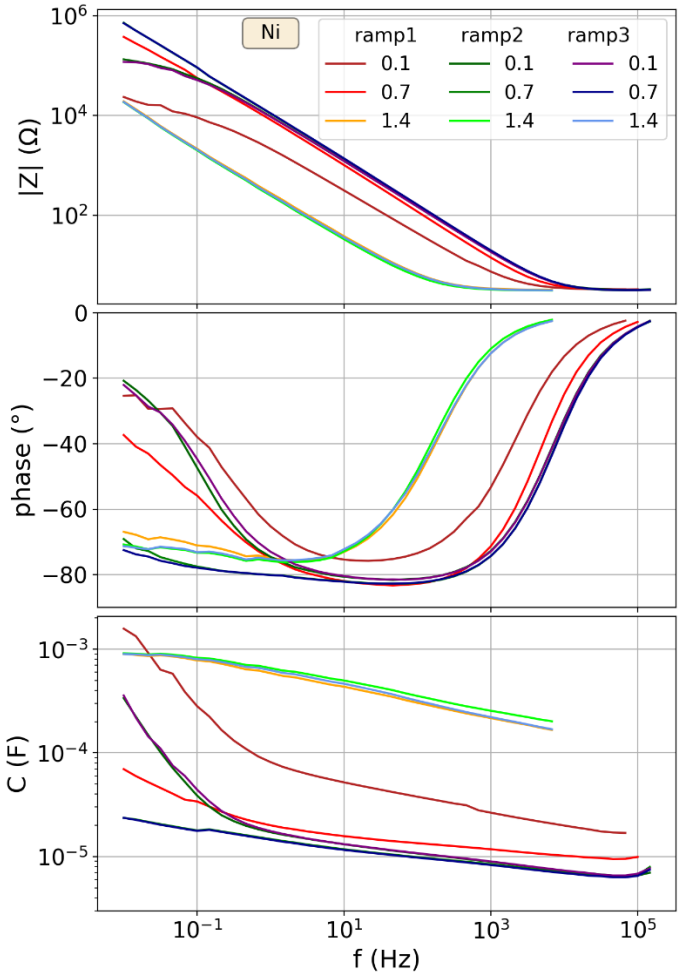

Figure S16: Nine impedance spectra and capacitance dispersions of the Ni electrode, three for each potential ramp at potentials of 0.1, 0.7 and 1.4 V vs RHE.

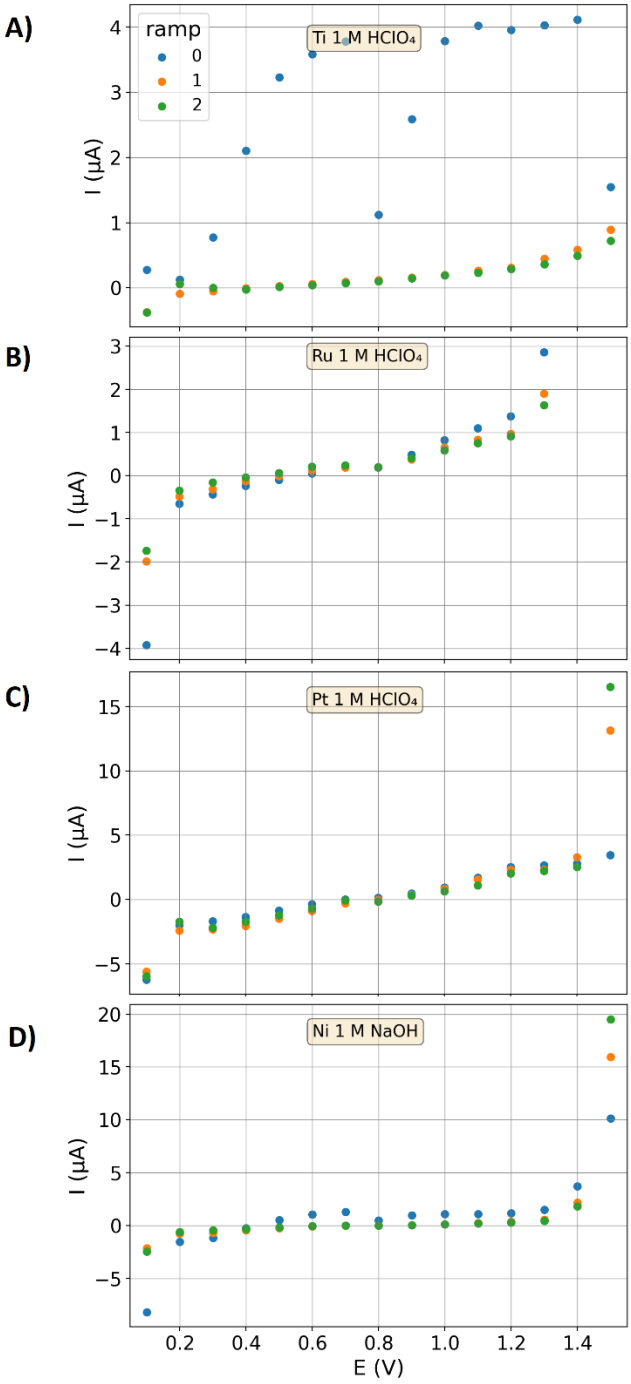

Figure S17: Bypass currents of the titanium (A), the ruthenium (B), the platinum (C) and the nickel specimen (D), recorded shortly before the impedance measurements at each potential step were started, respectively.